Project 2441 | April 2025

SJSU SAN JOSÉ STATE UNIVERSITY

MTI MINETA TRANSPORTATION INSTITUTE

Fuel Cell System Development for Heavy Duty Vehicles

Yu Yang, PhD Hen-Geul Yeh, PhD Bryan Aguirre

CSUTC California State University Transportation Consortium

CALIFORNIA STATE UNIVERSITY LONG BEACH

CSU TRANSPORTATION CONSORTIUM transweb.sjsu.edu/csutc

MINETA TRANSPORTATION INSTITUTE

Founded in 1991, the Mineta Transportation Institute (MTI), an organized research and training unit in partnership with the Lucas College and Graduate School of Business at San José State University (SJSU), increases mobility for all by improving the safety, efficiency, accessibility, and convenience of our nation's transportation system. Through research, education, workforce development, and technology transfer, we help create a connected world. MTI leads the Mineta Consortium for Emerging, Efficient, and Safe Transportation (MCEEST) funded by the U.S. Department of Transportation, the California State University Transportation Consortium (CSUTC) funded by the State of California through Senate Bill 1 and the Climate Change and Extreme Events Training and Research (CCEETR) Program funded by the Federal Railroad Administration. MTI focuses on three primary responsibilities:

Research

MTI conducts multi-disciplinary research focused on surface transportation that contributes to effective decision making. Research areas include: active transportation; planning and policy; security and counterterrorism; sustainable transportation and land use; transit and passenger rail; transportation engineering; transportation finance; transportation technology; and workforce and labor. MTI research publications undergo expert peer review to ensure the quality of the research.

Education and Workforce Development

To ensure the efficient movement of people and goods, we must prepare the next generation of skilled transportation professionals who can lead a thriving, forward-thinking transportation industry for a more connected world. To help achieve this, MTI sponsors a suite of workforce development and education opportunities. The Institute supports educational programs offered by the Lucas Graduate School of Business: a Master of Science in Transportation Management, plus graduate certificates that include High-Speed and Intercity Rail Management and Transportation Security Management. These flexible programs offer live online classes so that working transportation professionals can pursue an advanced degree regardless of their location.

Information and Technology Transfer

MTI utilizes a diverse array of dissemination methods and media to ensure research results reach those responsible for managing change. These methods include publication, seminars, workshops, websites, social media, webinars, and other technology transfer mechanisms. Additionally, MTI promotes the availability of completed research to professional organizations and works to integrate the research findings into the graduate education program. MTI's extensive collection of transportation-related publications is integrated into San José State University's world-class Martin Luther King, Jr. Library.

Report 25-06

Fuel Cell System Development for Heavy Duty Vehicles

Yu Yang, PhD

Hen-Geul Yeh, PhD

Bryan Aguirre

April 2025

A publication of the
Mineta Transportation Institute
Created by Congress in 1991

College of Business
San José State University
San José, CA 95192-0219

TECHNICAL REPORT DOCUMENTATION PAGE

1. Report No. 25-06	2. Government Accession No.	3. Recipient's Catalog No.
4. Title and Subtitle Fuel Cell System Development for Heavy Duty Vehicles		5. Report Date April 2025
		6. Performing Organization Code
7. Authors Yu Yang, PhD Hen-Geul Yeh, PhD Bryan Aguirre		8. Performing Organization Report CA-MTI-2441
9. Performing Organization Name and Address Mineta Transportation Institute College of Business San José State University San José, CA 95192-0219		10. Work Unit No.
		11. Contract or Grant No. SB1-SJAUX_2023-26
12. Sponsoring Agency Name and Address State of California SB1 2017/2018 Trustees of the California State University Sponsored Programs Administration 401 Golden Shore, 5th Floor Long Beach, CA 90802		13. Type of Report and Period Covered
		14. Sponsoring Agency Code

15. Supplemental Notes
10.31979/mti.2025.2441

16. Abstract
As California advances its ambitious goals for transportation electrification to combat climate change, hydrogen-powered fuel cells are emerging as a viable solution for overcoming the challenges of heavy-duty vehicles, offering an efficient alternative to lithium-ion batteries because they produce minimal chemical, thermal, and carbon emissions. One type of hydrogen fuel cell technology called proton exchange membrane fuel cells (PEMFCs) has garnered the most attention due to its distinct advantages, including relatively low operating temperatures (60–80 °C) and reliable performance at high current densities. However, despite their promise, PEMFCs face challenges, including in optimizing stack power output and safety concerns. To tackle these issues, accurate modeling and control strategies are essential. This study focuses on using data-driven modeling (specifically using a process known as "closed-loop system identification" under proportional controller and pseudo-random binary sequence excitation methods) to better understand and manage PEMFC systems. Various transfer functions models were analyzed, including first-order, first-order plus time delay, second-order, and second-order plus time delay models. The resulting closed-loop identification approach was applied on the humidifier, cooling, and oxygen supplier subsystems of simulated PEMFC to build their models under controlled operations. The results of this study highlight the potential of closed-loop system identification techniques to improve fuel cell vehicle performance in power supply, water, and heat management, without interrupting PEMFC operations. These findings demonstrate the significance of precise modeling as a cornerstone for advancing PEMFC control strategies and optimizing their application in renewable transportation and a more sustainable future.

17. Key Words Fuel cells, cooling, humidity, transfer functions, hydrogen.	18. Distribution Statement No restrictions. This document is available to the public through The National Technical Information Service, Springfield, VA 22161.		
19. Security Classif. (of this report) Unclassified	20. Security Classif. (of this page) Unclassified	21. No. of Pages 45	22. Price

Form DOT F 1700.7 (8-72)

DOI: 10.31979/mti.2025.2441

Mineta Transportation Institute
College of Business
San José State University
San José, CA 95192-0219

Tel: (408) 924-7560
Fax: (408) 924-7565
Email: mineta-institute@sjsu.edu

transweb.sjsu.edu/research/2441

ACKNOWLEDGMENTS

The authors are grateful for the administrative support from California State University, Long Beach (CSULB) and the College of Engineering. The authors also thank CSULB students for their technical contributions. This project is financially supported by the Mineta Transportation Institute at San José State University. The authors thank Lisa Rose and Editing Press for editorial services, as well as MTI staff Project Assistant Rajeshwari Rajesh and Graphic Design Assistant Katerina Earnest.

Contents

List of Figures

List of Tables

Executive Summary

California has set an ambitious goal to promote the adoption of electric vehicles in the transportation sector. While light-duty vehicles have made significant progress in electrification, heavy-duty vehicles face greater challenges in adopting lithium-ion battery technology due to their high weight and long charging times. These challenges can be effectively addressed by using fuel cell as an alternative power source. Consequently, integrating fuel cell systems into vehicles and regulating their power supply have emerged as urgent research topics.

As the first step, the research team studied the proton exchange membrane fuel cells (PEMFCs) in Simulink to develop its data-driven model. As an alternative, one may consider building a mechanism-based or machine learning model for PEMFCs. However, mechanism-based models usually require deep knowledge of reaction kinetics, fluid mechanics, heat/mass transfer, and electrochemistry. Machine learning models, such as neural network, demand a large volume of datasets and often lack interpretability. In contrast, the proposed method does not need sophisticated knowledge of the entire fuel cell system and can quickly capture the dynamic change of the system. In addition, the proposed method only uses a simple transfer function within a closed-loop framework. It requires only a modest dataset for parameter identification, avoids excessive computational demands, and can be easily implemented online.

This work yields the following discoveries:

- Closed-loop identification proves particularly effective for the hydrogen powered fuel cell system modeling with critical safety concerns.
- First-order, first-order plus time delay, second-order, and second-order plus time delay transfer functions are sufficiently accurate to model the subcomponents (humidifier, cooling, and oxygen supplier) of fuel cell systems.
- Data collected during vehicle start-up processes are highly valuable for modeling subcomponents.

1. Introduction

The development of renewable energy technologies continues to advance as a viable alternative to fossil fuels, addressing pollution and climate change. Among these technologies, hydrogen fuel cells stand out as a particularly promising solution for clean energy production, depending on whether the hydrogen is sourced from renewable or non-renewable processes [1]. Fuel cells are electrochemical devices that convert chemical energy directly into electricity through electrochemical reactions, producing only water and heat as byproducts. This environmentally friendly feature makes fuel cells highly attractive for reducing carbon emissions, as they produce minimal thermal, chemical, and carbon dioxide emissions [1]. While most fuel cell designs share a similar structure, they differ based on the type of electrolyte and fuel used. Proton Exchange Membrane Fuel Cells (PEMFCs) attract significant attention due to their numerous advantages, including low operating temperatures, high current density operation, lightweight and compact design, potential cost efficiency, long stack life, and suitability for intermittent operation.

The Membrane Electrode Assembly (MEA) is the core component of a Proton Exchange Membrane Fuel Cell (PEMFC). It consists of a proton exchange membrane sandwiched between an anode and a cathode, where electrochemical redox reactions generate power. The electrodes in the MEA typically include a gas diffusion layer made of carbon or cloth and a catalyst layer. Platinum (Pt) serves as the primary catalyst at the cathode, while a platinum-ruthenium (Pt-Ru) alloy is used at the anode to enhance reaction efficiency. Bipolar plates play a critical role by distributing reactant gases across the electrode surfaces via flow channels, collecting current, and providing structural support for the cell. Current collector plates then transmit the electrical current from the anode to the cathode through an external load, enabling power generation [1]. In the presence of Pt, the hydrogen oxidation reaction at the anode is given by

$$H_2 \rightarrow 2H^+ + 3e^-$$

and the oxygen reduction reaction at the cathode is

$$4H^+ + 4e^- + O_2 \rightarrow 2H_2O$$

The overall reaction of the PEMFC is given by

$$2H_2 + O_2 \rightarrow 2H_2O$$

Electrochemical reactions are fundamental to PEMFC operations, as they explain how the fuel cell generates electricity. The system's efficiency, power output, and overall performance depend on the rate and precise control of these reactions.

Most applications of PEMFC systems require high voltage and current. To meet these demands, multiple PEMFC cells are typically stacked and connected in series or parallel configurations to increase voltage and current output. However, this approach introduces challenges. Polarization phenomena at the electrodes can reduce voltage, compromising the performance of devices that require stable voltage levels [1]. Additionally, excessive heat generated during operations can weaken and eventually damage the membrane. Improper humidification may lead to electrode flooding, further reducing performance. Addressing these issues demands advanced control strategies to optimize power generation and ensure reliable PEMFC operation.

PEMFC systems can be divided into three key subsystems: reaction, thermal, and water management, as illustrated in Fig. 1. Each subsystem impacts the fuel cell's overall performance. To enhance performance, various control strategies have been explored, including optimizing electrochemical reactions within the stack and maintaining stable system voltage output despite voltage drops. These strategies rely on precise control of parameters such as humidity, temperature, and flow rate.

Figure 1. PEMFC System and Control Functions

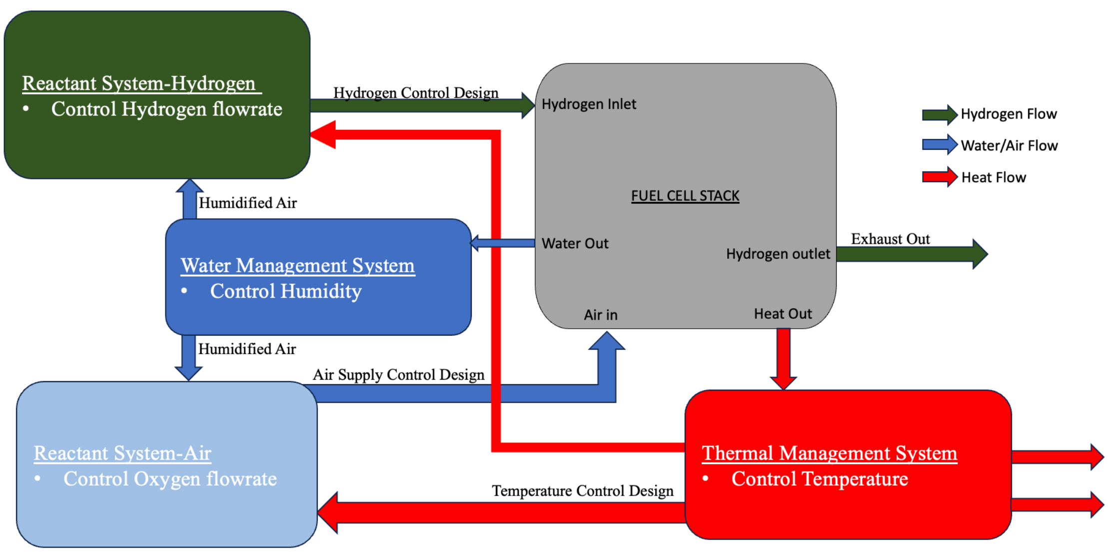

The reactant system in a PEMFC is responsible for supplying hydrogen to the anode and air to the cathode at a specific stoichiometric ratio. Maintaining the proper inlet pressure is essential to achieving the required airflow rate and sustaining the desired hydrogen-to-air ratio [1]. Managing pressure and flow rate within the stack can be challenging. High pressure can enhance reaction kinetics, increasing power density and efficiency, but reducing the net output power. Conversely, low pressure can cause voltage drops, increasing current density and risking damage to the stack. Although systems can be designed to deliver fixed reactant amounts and ratios, they often struggle to adapt to variable load demands [1]. Therefore, implementing an advanced reactant management system is crucial for optimizing PEMFC performance, durability, and adaptability under dynamic operating conditions.

The thermal management system plays a critical role in ensuring optimal operation and extending the lifespan of the PEMFC stack. Its primary function is to maintain the stack temperature within an appropriate range to support efficient electrochemical reactions. During operations, temperature variations across the PEMFC subsystems can significantly impact reaction rates and influence water evaporation and condensation in the reactant gases. While higher temperatures enhance electrochemical reaction rates, excessive or unstable temperatures can damage the membrane, causing voltage drops, electrode flooding, and reduced system performance and efficiency [1]. To prevent these issues, the optimal temperature range for low-temperature PEMFC designs is typically between 65°C and 85°C, as this range supports stable reactions while minimizing membrane degradation. Since a significant portion of the energy generated is released as heat, a well-designed thermal management system is essential to ensure uniform temperature distribution throughout the fuel cell stack.

The water management system is critical for maintaining proper hydration of the membrane and ensuring the appropriate water balance within the PEMFC. Water, a byproduct of the reaction, plays a vital role in facilitating proton transport through the membrane. A well-hydrated membrane enhances stability, prevents drying, and improves conductivity. Moreover, temperature significantly influences water levels. At low temperatures, inefficient water evaporation can lead to flooding, adversely affecting system performance. Water management strategies typically involve either external or internal humidification [1]. External humidification adjusts the humidity of reactant gases by controlling their temperature and contact time with water, while internal humidification directly introduces water into the PEMFC to hydrate the membrane and maintain optimal moisture levels. Designing an efficient water management system is essential to prevent flooding, sustain membrane hydration, and improve overall PEMFC performance.

1.1 Project Objective

The primary goal of this project is to perform closed-loop identification of PEMFC subsystems and develop transfer function models to support operational system design. The focus is specifically on the system modeling via closed-loop identification, rather than controller tuning. Our approach ensures the development of accurate models while avoiding additional open-loop unsafe step tests. In the closed-loop identification process, a proportional (P) controller is used instead of a step change. The P controller enables system observation under realistic and controlled conditions, which is crucial for building accurate models without interrupting system operations. Proportional-integral (PI) and proportional-integral-derivative (PID) controllers are not considered at this stage, because if accurate models can be constructed using data from the P controller, standard internal model control (IMC) tuning rules can later be applied to design effective PI or PID controllers.

A PEMFC model system developed using a custom Simscape block in MATLAB/Simulink [2] serves as the research testbed in this project. In this simulation, the fuel in the anode network comprises nitrogen, water vapor, and hydrogen, stored in a 70 MPa fuel tank. A pressure-reducing valve regulates hydrogen release to the stack at approximately 0.16 MPa, with unused hydrogen recirculated back to the stack. The cathode network, representing air from the environment, contains nitrogen, water vapor, and oxygen. An air compressor introduces air at a controlled rate, and a back-pressure relief mechanism maintains the pressure at around 0.16 MPa, venting exhaust to the environment. To ensure optimal operation under varying loads, the system maintains the temperature at 80°C and relative humidity at 1. A cooling system is incorporated to dissipate excess heat, while humidifiers saturate the gases with water vapor to keep the membrane well-hydrated. This comprehensive design ensures the stability and efficiency of the PEMFC under different operating conditions. The simulated system is illustrated in Fig. 2.

Figure 2. PEMFC Simulink Layout

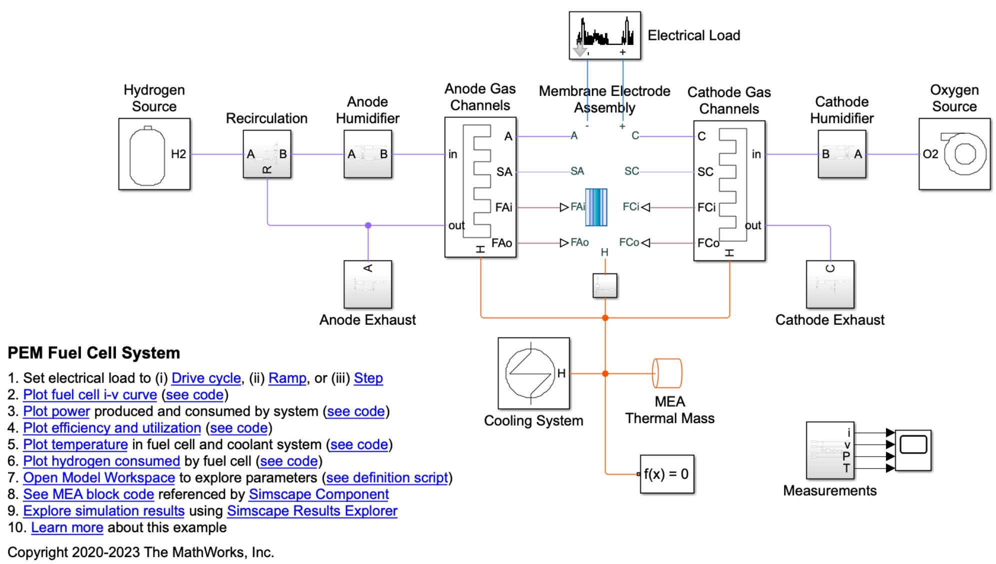

1.2 Background and Literature Review

Mathematical models of dynamical systems are crucial in engineering system designs. If the physical laws governing the behavior of the system are known, then a white box model can be constructed in which all the parameters and variables are known beforehand. Otherwise, a black box or grey box model, identified from data without exact knowledge of the system, can be constructed, and its parameters can be tuned to better fit the data.

System identification is a reliable technique useful for explaining the relation between the input and output of the system [3]. It can help build mathematical models from the data being generated, precisely when there is not enough information or when only a few system properties are known. The purpose of this technique is to create a visual representation of the actual process in a much simpler format. System identification can be divided into several subproblems such as experimental design, data collection, model structure selection, model estimation, and model validation. Experimental design involves choosing which signals to measure, sampling time, and excitation signals. Once this is done, the identification process can then be performed with the data that is generated. If the model structure is selected properly, the actual estimation of the parameters can be obtained accurately [3].

Fuel cell systems rely on feedback control to ensure safe operation and stable behavior. In an open-loop structure, there is no feedback mechanism; the output does not influence or modify the input, as the input is determined independently of the output. This makes open-loop systems less effective at compensating for disturbances. In contrast, a closed-loop system incorporates a feedback controller, which uses the output to adjust the input and maintain a stable process. The difference between the desired input (set point) and the feedback output generates an error signal, prompting a correction step to reduce the deviation. The primary function of a closed-loop system is to minimize this error and quickly restore the system to its set point. Closed-loop identification is particularly valuable because it allows system modeling without disrupting ongoing processes. This enables the development of accurate models while maintaining system operations. An example of a closed-loop system is shown in Fig. 3.

Figure 3. Closed-loop System with Disturbance Introduced

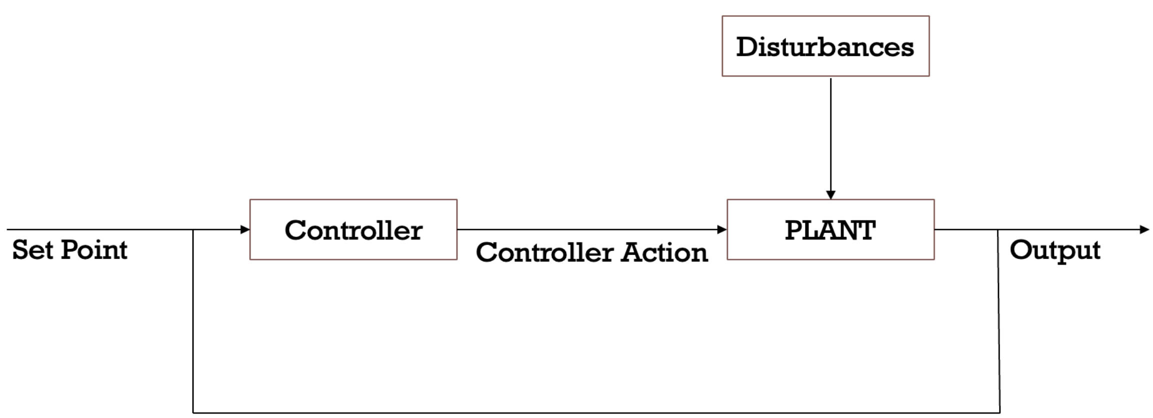

A significant challenge in closed-loop identification is that many identification methods effective in open-loop systems fail when applied directly to closed-loop input and output data. This limitation is evident in methods such as instrumental variables, spectral analysis, and various subspace techniques. Forssell attributes this failure to the non-zero correlation between the input and the unmeasured output noise inherent in closed-loop systems [3].

Another issue with closed-loop data is the potential loss of identifiability, which makes it difficult to uniquely determine system parameters from the measured input-output data [3]. Among the methods suitable for closed-loop systems, the prediction error method stands out as the most effective choice, as it can be applied directly to closed-loop data while addressing these challenges.

Closed-loop identification methods can be broadly categorized into three approaches—direct, indirect, and joint input-output—depending on the assumptions made about the feedback mechanism [4]. In the **direct approach**, the method is applied directly to measured input-output data without any assumptions about how the data was generated. This category includes methods such as the prediction error method and certain subspace techniques, which account for the correlation between input and noise. The **indirect approach** assumes complete knowledge of the feedback controller. In this method, the closed-loop system is identified first, and the open-loop parameters are derived from the estimate using the known controller dynamics. The **joint input-output approach** models both the input and output simultaneously, considering the output as being influenced by both the reference signal and noise [4]. While this approach does not require prior knowledge of the feedback controller, the controller must have a specific structure for the method to be effective. Both the indirect and joint input-output methods are typically applied to systems with linear feedback. They can also be extended to nonlinear feedback systems, but this significantly increases complexity. This study will focus on the indirect approach as the P controller can be easily integrated into the fuel cell system.

2. Closed-Loop Identification Methodology

In this section, we outline the closed-loop identification methodology. To evaluate the ability to estimate model parameters, a series of synthetic simulations were conducted to emulate the PEMFC system. These simulations represent a closed-loop system where the input signal combines a step function and a pseudo-random binary sequence (PRBS). PRBS, which mimics the behavior of a truly random sequence, is ideal for system identification as it efficiently excites the system across a broad frequency range. This ensures unbiased and accurate model identification, making it particularly suitable for capturing system dynamics. The simulation includes a proportional (P) controller block and a transfer function block that represents the synthetic process. The transfer functions tested for the process include first-order, first-order with time delay, second-order, and second-order with time delay (SOPTD) models. Key system parameters such as gain, time constant, time delay, and damping coefficient are estimated using the overall closed-loop transfer function derived from Equation (1):

$$G(s) = \frac{G_p(s)*G_c(s)}{1+G_p(s)*G_c(s)} \qquad (1)$$

where $G_p(s)$ represents the process model, and $G_c(s)$ represents the P controller. $G(s)$ represents the overall closed-loop transfer function of the system.

2.1 First-Order Model

The first type of model is the first-order transfer function, with the closed-loop control diagram shown in Fig. 4. The process setpoint is a step function plus PRBS signal. The output and input data are recoded and interpolated through the IDDATA Sink block.

Figure 4. First-Order Closed-Loop Simulation

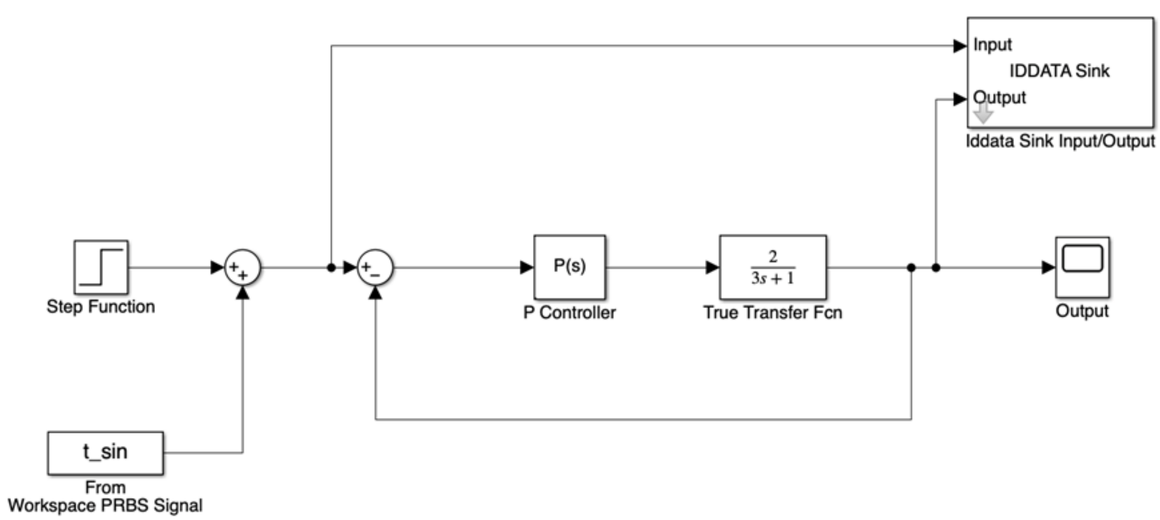

The overall closed-loop transfer function for the system can then be derived by using the formula shown in (1):

$$G_p(s) = \frac{K}{\tau s+1} \tag{2}$$

$$G_c(s) = K_c \tag{3}$$

$$G(s) = \frac{\frac{K*K_c}{1+K*K_c}}{\frac{\tau s}{1+K*K_c}+1} \tag{4}$$

where $G_p(s)$ represents the process model of the system, which in this case is a first-order transfer function as shown in equation (2). The transfer function contains two parameters. K in the numerator represents the process gain. τ in the denominator is the time constant of the process. $G_c(s)$ is the P controller with gain K_c shown in equation (3). The overall closed-loop transfer function of the system is then given by equation (4), which is the result of substituting (2) and (3) into equation (1).

From the simulation we have been able to generate input and output data based on the input of the process which is the step function added to the PRBS signal and the response to this change is the output. Using the system identification toolbox in MATLAB, this data can then be used to estimate a first-order closed-loop model, shown in Eq. (5):

$$G_{EP}(s) = \frac{K_p}{T_{p1}*s+1} \tag{5}$$

where $G_{EP}(s)$ in Eq. (5) represents the estimated first-order closed-loop model. Parameters K_p and T_{p1} in Eq. (5) are the estimated gain and time constants, respectively, for the closed-loop model. The best model fit for the estimated first-order closed-loop model is displayed in Fig. 5.

As Eq. (4) and (5) are equal, the parameters, such as gain and time constant, can be estimated accordingly:

$$G(s) = G_{EP}(s) = \frac{\frac{K*K_c}{1+K*K_c}}{\frac{\tau}{1+K*K_c}*s+1} = \frac{K_p}{T_{p1}*s+1} \tag{6}$$

$$\frac{K*K_c}{1+K*K_c} = K_p \Rightarrow K = \frac{K_p}{(1-K_p)K_c} \tag{7}$$

$$\frac{\tau}{1+K*K_c} = T_{p1} \Rightarrow \tau = T_{p1}(1+K*K_c) \tag{8}$$

where Eq. (6) implies that two transfer functions have the same gain and time constant, and thus Eqs. (7)–(8) hold. In this study, we vary the controller gain and obtain different response datasets to estimate the process parameters K and τ by using Eqs. (7)–(8). The results are shown in Table 1.

Figure 5. Best Fit for Estimated Firs-Order Closed-Loop Model with P = 0.1

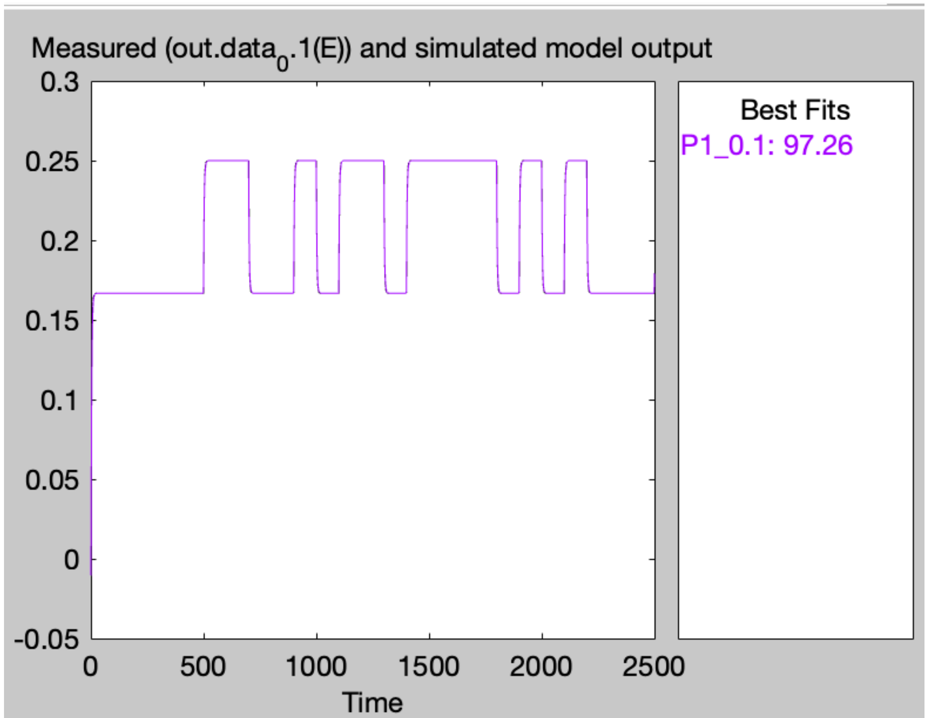

Table 1. Estimated Parameters for First-Order Process Based on P Controller Range 0.1–1

P Controller Gain	Estimated Gain K_p in Closed Loop	Estimated Time constant τ_{p1} sec in Closed Loop	Estimated K gain	Estimated Time constant τ sec
0.1	0.16669	2.9768s	2.0004	3.5723s
0.2	0.28575	2.6246s	2.0004	3.6741s
0.3	0.37505	2.3919s	2.0004	3.8273s
0.4	0.4445	2.1838s	2.0004	3.9312s
0.5	0.50006	2.0164s	2.0004	4.0333s
0.6	0.54552	1.8784s	2.0005	4.1331s
0.7	0.5834	1.762s	2.0005	4.2295s
0.8	0.5834	1.762s	2.0006	4.2295s
0.9	0.64294	1.5743s	2.0007	4.4091s
1	0.66675	1.4964s	2.0008	4.4903s

From Figure 4, we know that the true value of gain is $K = 2$ and the time constant is $\tau = 3$. Comparing true values with the estimation shown in Table 1, we can conclude that when controller gain is reduced, the estimation accuracy can be improved.

2.2 First-Order Plus Time Delay (FOPTD) Model

The second simulation is based on a first-order process plus time delay (FOPTD) model, and the control diagram is shown in Fig. 6. The input and output of the process remain the same, as does the true transfer function being used, but now a 5-second time delay is introduced.

Figure 6. FOPTD Closed-Loop Simulation (Time Delay=5 Seconds)

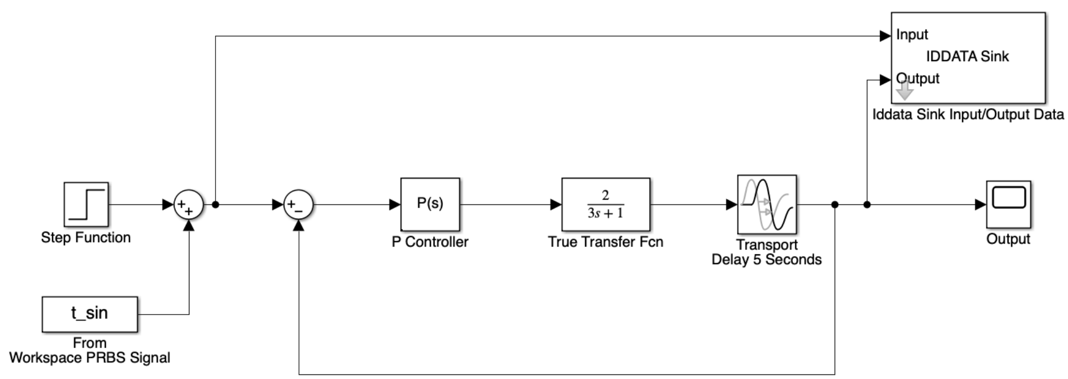

To handle the time delay term, we can employ the 1/1 páde approximation shown in Eq. (9):

$$e^{(-\theta s)} = \frac{1-\frac{\theta s}{2}}{1+\frac{\theta s}{2}} \qquad (9)$$

Then, the true process model can be approximated as:

$$G_p(s) = \frac{K}{\tau s+1} e^{(-\theta s)} \rightarrow G_p(s) \approx \frac{K}{\tau s+1} * \frac{1-\frac{\theta}{2}s}{1+\frac{\theta}{2}s} = \frac{K-\frac{K*\theta}{2}s}{\tau s+1+\frac{\theta}{2}s+\frac{\tau*\theta}{2}s^2} = \frac{K-\frac{K*\theta}{2}s}{\frac{\tau*\theta}{2}s^2+\left(\tau+\frac{\theta}{2}\right)s+1} \qquad (10)$$

The overall closed-loop transfer function for the FOPTD with P controller can be derived by substituting Eq. (10) into Eq. (1), which results in Eq. (11):

$$G(s) = \frac{K_C * \frac{K - \frac{K*\theta}{2}s}{\frac{\tau\theta}{2}s^2 + \left(\tau + \frac{\theta}{2}\right)s + 1}}{1 + K_C * \frac{K - \frac{K*\theta}{2}s}{\frac{\tau*\theta}{2}s^2 + \left(\tau + \frac{\theta}{2}\right)s + 1}} = \frac{\frac{K_C*K - \frac{K_C*K*\theta}{2}s}{\frac{\tau\theta}{2}s^2 + \left(\tau + \frac{\theta}{2}\right)s + 1}}{\frac{\frac{\tau*\theta}{2}s^2 + \left(\tau + \frac{\theta}{2}\right)s + 1 + K_C*K - \frac{K_C*K*\theta}{2}s}{\frac{\tau*\theta}{2}s^2 + \left(\tau + \frac{\theta}{2}\right)s + 1}} = \frac{\frac{K_C*K}{1+K*K_C} - \frac{\frac{K_C*K*\theta}{2}s}{1+K*K_C}}{\frac{\frac{\tau*\theta}{2}s^2}{1+K_C*K} + \frac{\left(\tau + \frac{\theta}{2} - \frac{K_C*K*\theta}{2}\right)s}{1+K_C*K} + 1} \qquad (11)$$

Because Eq. (11) is a second-order process model, we can use MATLAB System Identification App to identify its parameters:

$$G_{EP}(s) = \frac{K_p + (K_p * T_z)s}{(T_{p1} * T_{p2})s^2 + (T_{p1} + T_{p2})s + 1} \qquad (12)$$

where $G_{EP}(s)$ in Eq. (12) represents the estimated closed-loop model. The best model fit for the estimated FOPTD model is illustrated in Fig. 7.

Figure 7. Best Fit for Estimated FOPTD Closed-Loop Model with P = 0.1

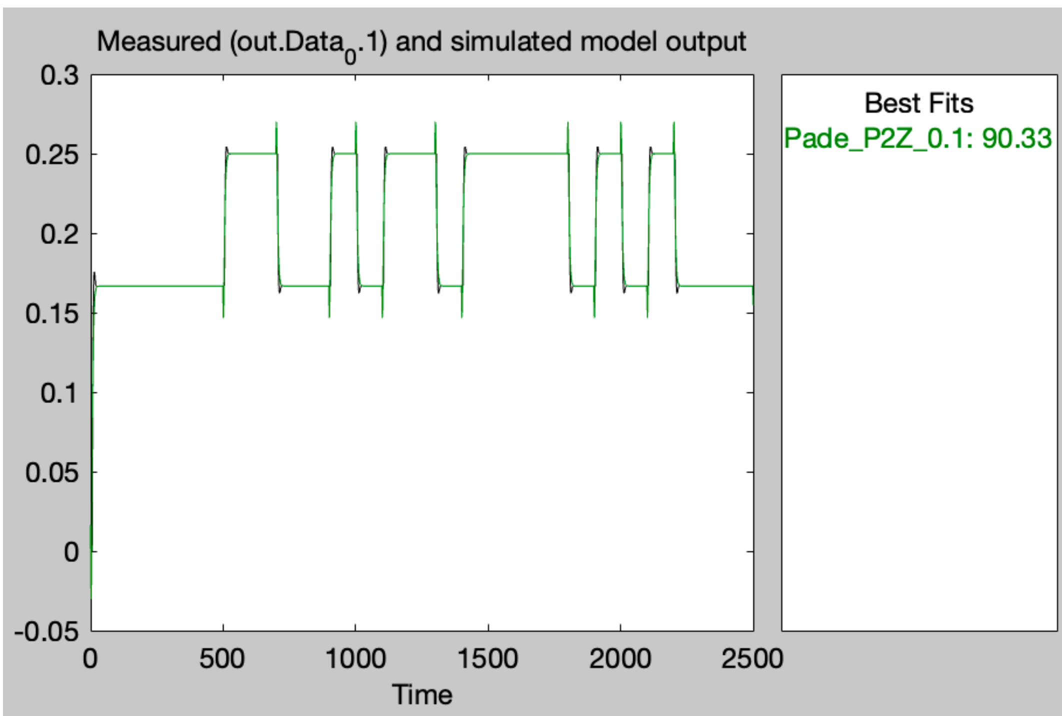

Using the estimated closed-loop model (12) along with the overall closed-loop transfer function (11), the parameters of gain and time delay can be estimated uniquely, as shown in (13)–(17):

$$G(s) = G_{EP}(s) \rightarrow \frac{\frac{K_C*K}{1+K*K_C} - \frac{\frac{K_C*K*\theta}{2}s}{1+K*K_C}}{\frac{\frac{\tau*\theta}{2}s^2}{1+K_C*K} + \frac{\left(\tau + \frac{\theta}{2} - \frac{K_C*K*\theta}{2}\right)s}{1+K_C*K} + 1} = \frac{K_p + (K_p * T_z)s}{(T_{p1} * T_{p2})s^2 + (T_{p1} + T_{p2})s + 1} \qquad (13)$$

$$\frac{Kc*K}{1+K*Kc} = K_p \ \Rightarrow K = \frac{K_p}{(1-K_p)K_c} \tag{14}$$

$$\frac{\frac{Kc*K*\theta}{2}}{1+K*Kc} = K_p * -T_z \ \Rightarrow \ \theta = \frac{(K_p*(-T_z)\,)*2(1+K*Kc)}{Kc*K} \tag{15}$$

$$\frac{\frac{\tau*\theta}{2}}{1+Kc*K} = \ T_{p1} * T_{p2} \tag{16}$$

$$\frac{\left(\tau+\frac{\theta}{2}-\frac{Kc*K*\theta}{2}\right)}{1+Kc*K} = T_{p1} + T_{p2} \tag{17}$$

However, the time constant is more complex because solving Eqs. (16) and (17) may generate two values of τ:

$$\tau_1 \ = \frac{(T_{p1}*T_{p2})*2(1+Kc*K)}{\theta} \tag{18}$$

$$\tau_2 = \left(T_{p1} + T_{p2}\right) * (1 + Kc * K) - \frac{\theta}{2} + \frac{Kc*K*\theta}{2} \tag{19}$$

To resolve this issue, we will use the average of τ_1 and τ_2 as the identified time constant. In Table 2, we show the estimation results by varying the controller gain from 0.01 to 0.5.

Table 2. Estimated Parameters for FOPTD

P Controller	Estimated K gain	Estimated Time delay θ sec	Estimated τ_1 sec	Estimated τ_2 sec	Average τ
0.01	2.0003	5.5248s	3.7286s	3.7754s	3.7520s
0.02	2.0002	5.4624s	3.5597s	3.7380s	3.6488s
0.03	1.9999	5.5230s	3.5356s	3.8383s	3.6869s
0.04	1.9999	5.6242s	3.3844s	3.8249s	3.6047s
0.05	2.0007	5.2882s	3.6825s	4.1741s	3.9283s
0.1	2.0005	5.8878s	2.8156s	4.0276s	3.4216s
0.2	2.0015	5.3248s	3.1264s	5.2317s	4.1790s
0.3	2.0024	5.0526s	3.4807s	6.4948s	4.9878s
0.4	1.9995	6.4108s	2.7398s	7.3099s	5.0249s
0.5	2.0013	7.0578s	2.3392s	8.1301s	5.2346s

The true transfer function model being used for the FOPTD has a gain of 2, a time constant of 3, and a time delay of 5 seconds. Based on Table 2, for the most part the estimated gain does remain close to its true value. The time delay, on the other hand, strays away from the true value as the P controller gain continues to increase. In this case, since we have estimated two-time constants, we decided to use the average of both, which is close to 3 but varies based on the value of the P controller. Overall, P = 0.1 still leads to a more accurate estimation than other values of the gain.

2.3 Second-Order Model

The third simulation is a second-order overdamped process. The input and output to the process remain the same as previous sections. The true transfer function being introduced is second-order, and the control diagram can be seen in Fig. 8.

Figure 8. Second-Order Closed-Loop Simulation

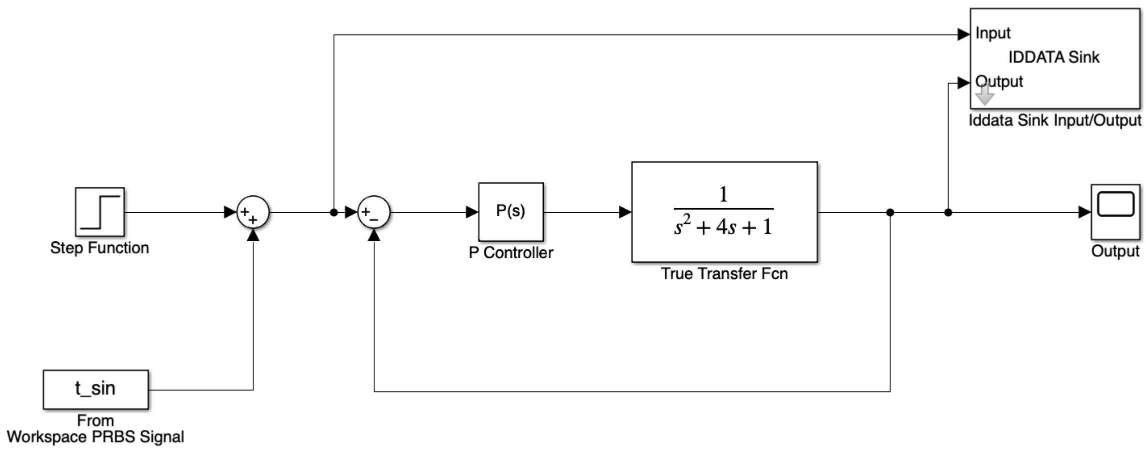

The process model is shown in Eq. (20):

$$G_p(s) = \frac{K}{\tau^2 s^2 + 2*\zeta*\tau s + 1} \tag{20}$$

where the damping coefficient ζ represents the degree of oscillation in response to the disturbance. Then, the closed-loop transfer function in Fig. 7. can be derived:

$$G(s) = \frac{\frac{K}{\tau^2 s^2+2*\zeta*\tau s+1}*K_C}{1+\frac{K}{\tau^2 s^2+2*\zeta*\tau s+1}*K_C} = \frac{\frac{K*K_C}{\tau^2 s^2+2*\zeta*\tau s+1}}{\frac{\tau^2 s^2+2*\zeta*\tau s+1+K*K_C}{\tau^2 s^2+2*\zeta*\tau s+1}} = \frac{K*K_C}{\tau^2 s^2+2*\zeta*\tau s+1+K*K_C} = \frac{\frac{K*K_C}{1+K_C*K}}{\frac{\tau^2 s^2}{1+K_C*K}+\frac{2*\zeta*\tau s}{1+K_C*K}+1} \tag{21}$$

Note that Eq. (21) is still a second-order transfer function. We can use the system identification App to estimate its parameters. The results are shown in Fig. 9 with model structure in Eq. (22):

$$G_{EP}(s) = \frac{K_p}{(T_{p1}*T_{p2})s^2+(T_{p1}+T_{p2})s+1} \tag{22}$$

Then, we can estimate the process model parameters K, τ, and ζ:

Figure 9 Best Fit for Estimated Second-Order Closed-Loop Model with P = 0.1

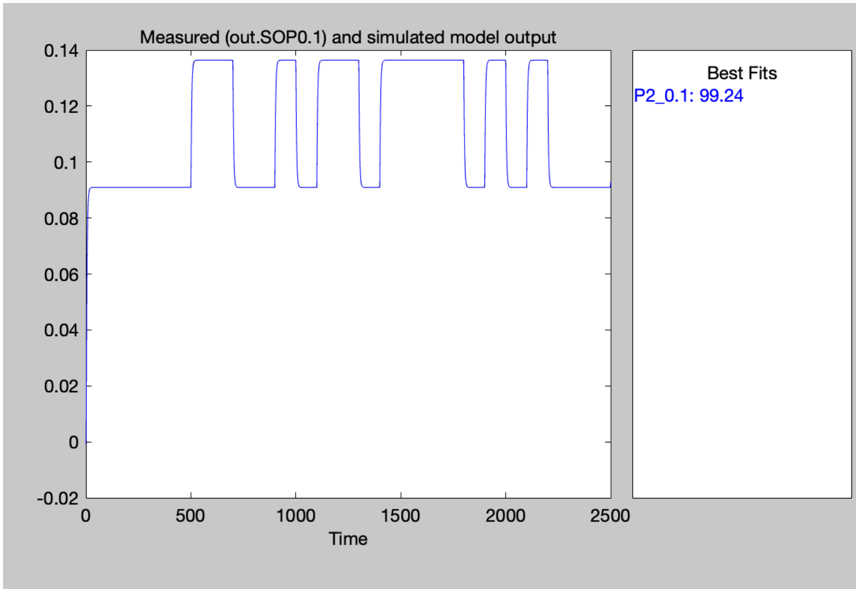

$$G(s) = G_{EP}(s) \Rightarrow \frac{\frac{K*K_c}{1+K_c*K}}{\frac{\tau^2 s^2}{1+K_c*K}+\frac{2*\zeta*\tau s}{1+K_c*K}+1} = \frac{K_p}{(T_{p1}*T_{p2})s^2+(T_{p1}+T_{p2})s+1} \tag{23}$$

$$\frac{K*K_c}{1+K_c*K} = K_p \Rightarrow K = \frac{K_p}{(1-K_p)K_c} \tag{24}$$

$$\frac{\tau^2}{1+K_c*K} = T_{p1} * T_{p2} \Rightarrow \tau = \sqrt{T_{p1} * T_{p2}(1 + K_c * K)} \tag{25}$$

$$\frac{2*\zeta*\tau}{1+K_c*K} = T_{p1} + T_{p2} \Rightarrow \zeta = \left(T_{p1} + T_{p2}\right)(1 + K_c * K)/2\tau \tag{26}$$

The true transfer function has a gain of 1, a time constant of 1, and a damping coefficient of 2. The estimated parameters obtained for the closed-loop model are displayed in Table 3 by varying the P controller gain from 0.1 to 3.

Table 3. Estimated Parameters for Second-Order Process Model

P Controller	Estimated Gain K	Estimated Tau τ sec	Estimated Damping Coefficient ζ
0.1	1.0000	1.7347s	1.2887
0.2	1.0000	1.7352s	1.2991
0.3	1.0000	1.7359s	1.3092
0.4	1.0000	1.7364s	1.3193
0.5	1.0000	1.7370s	1.3290
1	1.0000	1.7003s	1.4142
2	1.0002	1.5270s	1.7322
3	1.0004	1.4419	2.0003

Based on Tables 2 and 3, the observed trends highlight a key difference between first-order and second-order models. Increasing the P controller gain tends to reduce parameter estimation accuracy for the first-order process. However, in the second-order transfer function simulation, increasing the proportional gain improves the estimation accuracy of the time constant and damping coefficient. The most accurate parameter estimates for the second-order transfer function, compared to the true values used in the simulation, were obtained with a P controller gain of 3.

2.4 Second-Order Plus Time Delay Model

The last simulation is a second-order plus time delay process. A time delay of 2 seconds has been introduced. The true transfer function being applied in the simulation is still second-order, and the control block diagram is shown in Fig. 10.

Figure 10. Second-Order Plus Time Delay Simulation

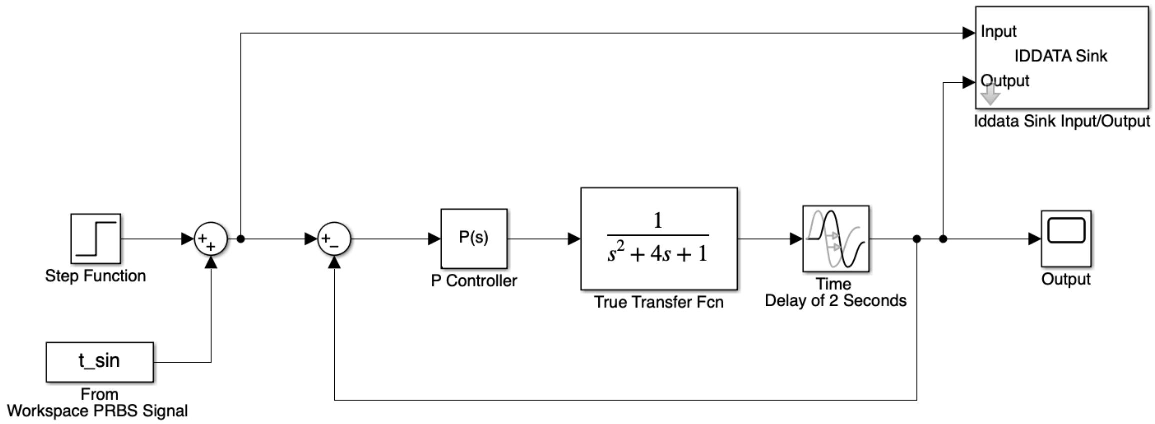

To deal with the time delay, a 1/1 páde approximation can be applied and a new process model is created in Eq. (27). Substituting Eq. (27) into Eq. (1), the overall closed-loop transfer function can be derived in Eq. (28):

$$G_p(s) = \frac{K*e^{-\theta s}}{\tau^2 s^2+2*\zeta*\tau s+1} = \frac{K-\frac{K*\theta s}{2}}{\frac{\tau^2*\theta}{2}s^3+(\tau^2+\zeta*\tau*\theta)s^2+\left(2*\zeta*\tau+\frac{\theta}{2}\right)s+1} \tag{27}$$

$$G(s) = \frac{\frac{\left(K-\frac{K*\theta s}{2}\right)*K_c}{\frac{\theta}{2}s^3+(\tau^2+\zeta*\tau*\theta)s^2+\left(2*\zeta*\tau+\frac{\theta}{2}\right)s+1}}{1+\frac{K_c*K-\frac{K_c*K*\theta s}{2}}{\frac{\tau^2\theta}{2}s^3+(\tau^2+\zeta*\tau*\theta)s^2+\left(2*\zeta*\tau+\frac{\theta}{2}\right)s+1}} = \frac{\frac{\left(K*Kc-\frac{Kc*K*\theta s}{2}\right)}{\frac{\tau^2*\theta}{2}s^3+(\tau^2+\zeta*\tau*\theta)s^2+\left(2*\zeta*\tau+\frac{\theta}{2}\right)s+1}}{\frac{\frac{\tau^2*\theta}{2}s^3+(\tau^2+\zeta*\tau*\theta)s^2+\left(2*\zeta*\tau+\frac{\theta}{2}-\frac{Kc*K*\theta}{2}\right)s+1+Kc*K}{\frac{\tau^2\theta}{2}s^3+(\tau^2+\zeta*\tau*\theta)s^2+\left(2*\zeta*\tau+\frac{\theta}{2}\right)s+1}} =$$

$$\frac{\left(K_c*K-\frac{K_c*K*\theta s}{2}\right)}{\frac{\tau^2*\theta}{2}s^3+(\tau^2+\zeta*\tau*\theta)s^2+\left(2*\zeta*\tau+\frac{\theta}{2}-\frac{K_c*K*\theta}{2}\right)s+(1+K_c*K)} = \frac{\frac{\left(K_c*K-\frac{K_c*K*\theta s}{2}\right)}{1+Kc*K}}{\frac{\frac{\tau^2\theta}{2}s^3}{1+K_c*K}+\frac{(\tau^2+\zeta*\tau*\theta)s^2}{1+K_c*K}+\frac{\left(2*\zeta*\tau+\frac{\theta}{2}-\frac{K_c*K*\theta}{2}\right)}{1+K*K_c}s+1} \tag{28}$$

Eq. (28) is a third-order transfer function because of the 1/1 páde approximation, and the polynomial in the denominator must be set in standard form. From the equation, we can estimate the following parameters of gain K, time constant τ, time delay θ, and the damping coefficient ζ. Eq. (29) can be used to obtain the closed-loop model along with the best fit shown in Fig. 11:

$$G_{EP}(s) = \frac{K_p+(K_p*T_z)s}{(T_{p1}*T_{p2}*T_{p3})s^3+(T_{p1}+T_{p2}*T_{p3})s^2+(T_{p1}+T_{p2}+T_{p3})s+1} \tag{29}$$

Figure 11. Best Fit for Estimated Second-Order Plus Time Delay Closed-Loop Model with P = 0.1.

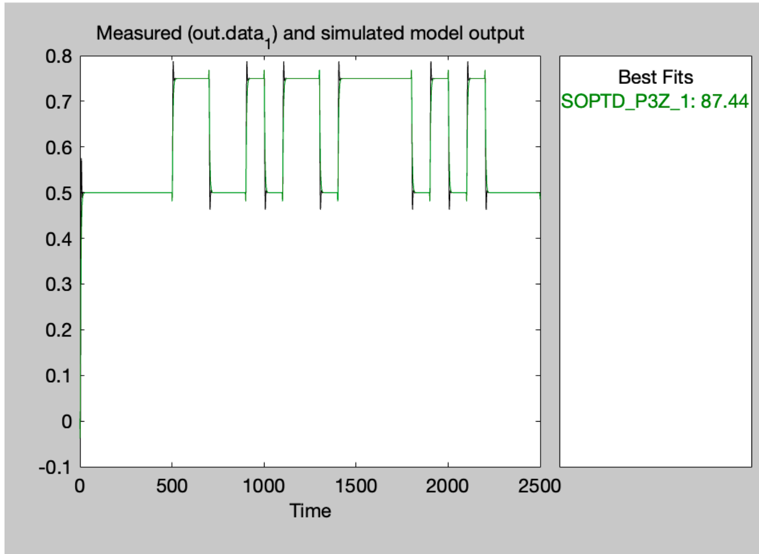

Then, we can derive the gain, time constant, damping coefficient, and time delay via Eqs. (30)–(35). Again, due to the approximation, there are two possible values for the time constant, denoted as τ_1 and τ_2.

$$G(s) = G_{EP}(s) \Rightarrow \frac{\frac{\left(K_C*K-\frac{K_C*K*\theta s}{2}\right)}{1+KcK}}{\frac{\frac{\tau^2*\theta}{2}s^3}{1+K_C*K}+\frac{(\tau^2+\zeta*\tau*\theta)s^2}{1+K_C*K}+\frac{\left(2*\zeta*\tau+\frac{\theta}{2}-\frac{K_C*K*\theta}{2}\right)}{1+K*K_C}s+1} =$$

$$\frac{K_p+(K_p*T_z)s}{(T_{p1}*T_{p2}*T_{p3})s^3+(T_{p1}+T_{p2}*T_{p3})s^2+(T_{p1}+T_{p2}+T_{p3})s+1} \quad (30)$$

$$\frac{K_c*K}{1+K_c*K} = K_p \Rightarrow K = \frac{K_p}{(1-K_p)K_c} \quad (31)$$

$$\frac{\frac{Kc*K*\theta}{2}}{1+Kc*K} = -K_p * T_z \Rightarrow \theta = \frac{(K_p*T_z)*2(1+K_c*K)}{K_c*K} \quad (32)$$

$$\frac{\frac{\tau^2*\theta}{2}}{1+Kc*K} = T_{p1} * T_{p2} * T_{p3} \Rightarrow \tau_1 = \sqrt{\frac{(T_{p1}*T_{p2}*T_{p3})*2(1+K_c*K)}{\theta}} \quad (33)$$

$$\frac{(\tau^2+\zeta*\tau*\theta)}{1+Kc*K} = (T_{p1} + T_{p2} * T_{p3}) \Rightarrow \zeta = \frac{(T_{p1}+T_{p2}*T_{p3})*1+Kc*K-\tau^2}{\tau*\theta} \quad (34)$$

$$\frac{\left(2*\zeta*\tau+\frac{\theta}{2}-\frac{K_C*K*\theta}{2}\right)}{1+K*K_c} = (T_{p1} + T_{p2} + T_{p3}) \Rightarrow \tau_2 = \frac{(T_{p1}+T_{p2}+T_{p3})*1+K*K_c-\frac{\theta}{2}+\frac{K_C*K*\theta}{2}}{2*\zeta} \quad (35)$$

The true transfer function has the gain as 1, the time constant as 1, the damping coefficient as 2, and the time delay as 2 seconds. In Table 4, we show the estimated parameters by varying controller gain from 0.1 to 1.5.

Table 4. Estimated Parameters for Second-Order Transfer Function Plus Time Delay

P controller gain	Estimated gain K	Estimated time delay θ sec	Estimated τ (based on avg of τ_1& τ_2)	Estimated damping coefficient ζ
0.1	1.0000	2.2302s	1.7661s	1.1538
0.2	1.0000	2.2250s	1.8360s	1.0628
0.3	1.0000	2.6834s	1.4878s	1.1914
0.4	1.0000	2.7998s	1.6979s	0.8412
0.5	1.0002	2.5024s	1.7531s	1.2642
1	0.9996	2.5472s	1.3623s	1.9392
1.5	1.0003	2.5428s	2.9690s	2.9813

Among all estimation results, when the P controller gain is set at 1, the estimation is the most accurate representation to the true transfer function of the simulation.

3. Closed-Loop System Identification of PEMFC Humidifier

The PEMFC model incorporates two humidifiers, one on the anode side and the other on the cathode side, both operating under identical conditions with a proportional (P) controller. The primary objective of the P controller is to maintain relative humidity at a safe level of 1 (100%). This chapter aims to model the humidifier and analyze the dominant dynamics of the system. To achieve this, a Pseudo-Random Binary Sequence (PRBS) signal is used to excite the input, enabling the generation of setpoint variations and output data for closed-loop model estimation. Controlling humidity poses a challenge due to its slow response to changes, and improper adjustments may destabilize the PEMFC system. In this study, the setpoint variations are introduced by replacing the original setpoint of 1 in the P controller with a PRBS signal. The PRBS signal introduces a ±5% disturbance from the setpoint and is labeled as "HumidifierInput" in the control diagram (Fig. 12). It is important to note that the relative humidity should not exceed 100%, and the perturbation signal is solely intended for identification purposes. The process output, representing the relative humidity measurement, is analyzed in response to the PRBS input. For consistency, the P controller gain was fixed at 0.1 across all models.

Figure 12. PEMFC Humidifier with PRBS Signal as Setpoint

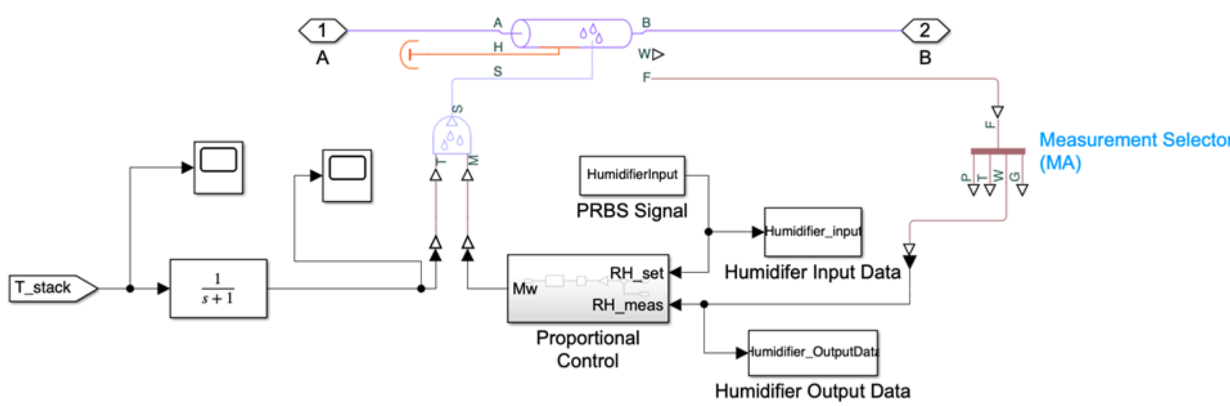

To safely model the humidifier in the PEMFC, we replace the fixed setpoint in the closed-loop system with a PRBS input. Input and output datasets are generated and preprocessed by removing the mean from datasets. The processed dataset is then interpolated to ensure consistent sampling intervals between the input and output signals. Using MATLAB's System Identification Toolbox, we estimate closed-loop models for the humidifier. Instead of predefining the model structure, we evaluate several options, including first-order, first-order with time delay, second-order, and second-order with time delay transfer functions. The data fitting results are shown in Fig. 13. "Humidifier_P1" represents the first-order model, "Humidifier_P2Z" represents the FOPTD model, "Humidifier_P2" represents the second-order model, and "Humidifier_P3Z" represents the second-order plus time delay model. Applying the formulas derived in Chapter 2, we can estimate model parameters, summarized in Table 5.

Based on the estimation results, the two best-performing models are first-order and FOPTD. The second-order and second-order plus time delay models exhibit excessively large damping coefficients and small time constants, resulting in a highly sensitive, inefficient, and impractical system for real-world applications. Additionally, the model fit for the estimated closed-loop models highlights the effectiveness of the estimation process. In this case, the low fit values indicate that the models struggle to capture the fluctuations occurring in the system. To potentially improve the model fit, techniques such as tuning the proportional (P) controller gain can be explored. However, for this analysis, the P controller gain was kept at 0.1 to avoid the risks associated with high-gain controllers, which can be too aggressive and may destabilize the system. Our comparison results show that the FOPTD is the best model with 59.96% accuracy.

Figure 13. Best Fit for Estimated Closed-Loop Models with PRBS as Humidity Setpoint with P = 0.1.

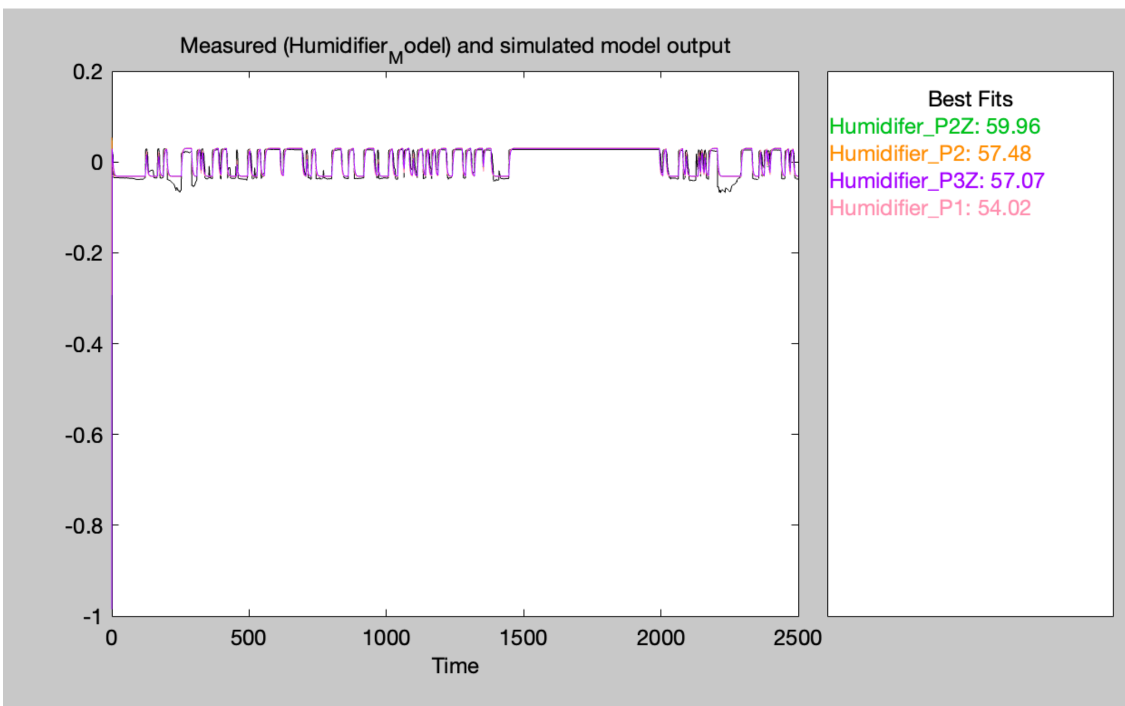

Table 5. Estimated Model Parameters for Humidifier System

Process Model	P Controller	Estimated Gain $\hat{K}$	Avg Time Constant τ sec	Time Delay θ sec	Damping Coefficient ζ	Model Fit %
First-Order	0.1	15.2781	5.2027s	N/A	N/A	54.02
FOPTD	0.1	16.6151	4.7486s	2.1296s	N/A	59.96
Second-Order	0.1	16.6085	0.1136s	N/A	37.3720	57.48
Second-Order Plus Time Delay	0.1	16.0858	0.0629s	2.7936s	74.2251	57.05

The dataset in Fig. 13 contains a big step change in the initial time point, which represents the humidifier system start-up. To investigate the impact of start-up on system modeling, we trim the dataset to eliminate the start-up section and rebuild the model. The resulting model fits are shown in Fig. 14 and parameters are listed in Table 6.

Figure 14. Best Fit for Estimated Closed-Loop Models Using Trimmed Input/Output with PRBS with P = 0.1

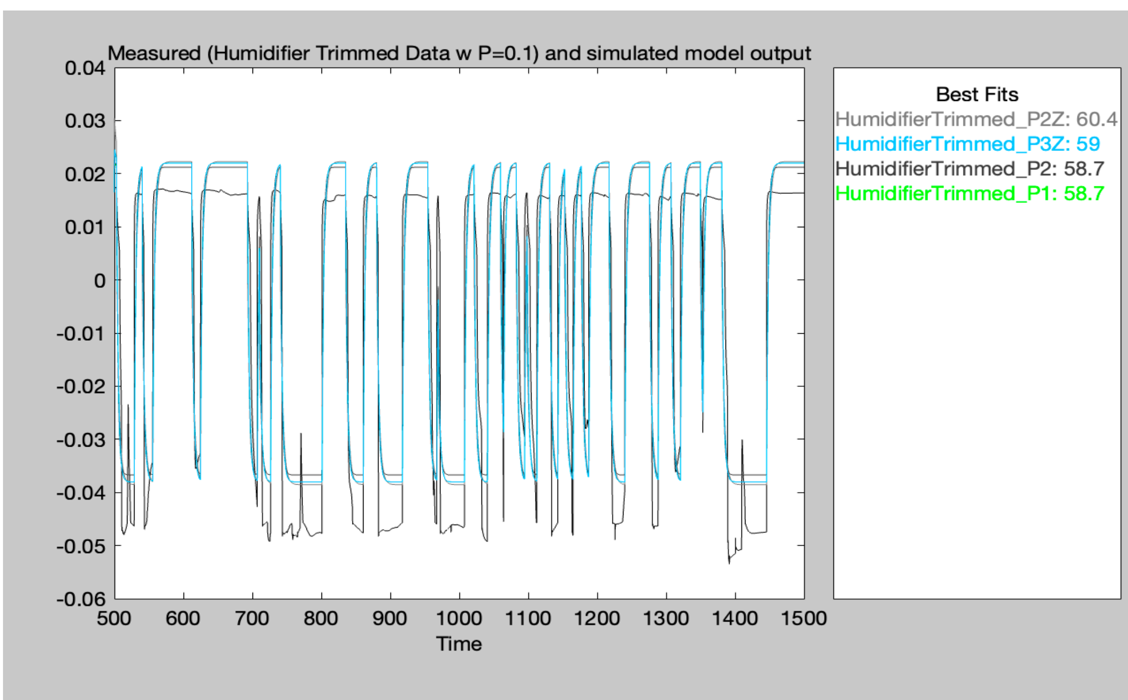

Table 6. Estimated Model Parameters Based on Trimmed Data for Humidifier System

Process Model	P Controller	Estimated Gain $\widehat{K}$	Avg Time Constant τ sec	Time Delay θ sec	Damping Coefficientζ	Model Fit %
First-Order	0.1	13.784	5.0975s	N/A	N/A	58.7
FOPTD	0.1	15.522	4.7417s	2.0554s	N/A	60.04
Second-Order	0.1	13.784	7.3546e-05s	N/A	3.465e+04	58.07
SOPTD	0.1	15.006	0.0045s	0.3345s	191.280	59.00

Table 6 demonstrates that the FOPTD model remains the best option among these low-order transfer functions. The model accuracy of FOPTD is only improved by 0.08% when the start-up data section is excluded. Additionally, three model parameters K, τ, and ζ do not change significantly between Tables 5 and 6. Therefore, we can draw two conclusions for this chapter:

- The PEMFC humidifier can be effectively modeled by a FOPTD.
- The inclusion of start-up data for the humidifier has minimal impact on the model accuracy, and thus can be kept in the closed-loop identification dataset safely.

4. Closed-Loop Identification of PEMFC Cooling System

The cooling system in the PEMFC serves several critical functions to ensure optimal performance, durability, and safety. The main role of this system is to absorb heat by circulating coolants through the cells and releasing it into the environment. The humidifiers are then responsible for saturating the gas with water vapor, keeping the membrane hydrated. Fig. 15 shows the diagram of the cooling system within the simulation.

Figure 15. PEMFC Cooling System with PRBS Setpoint

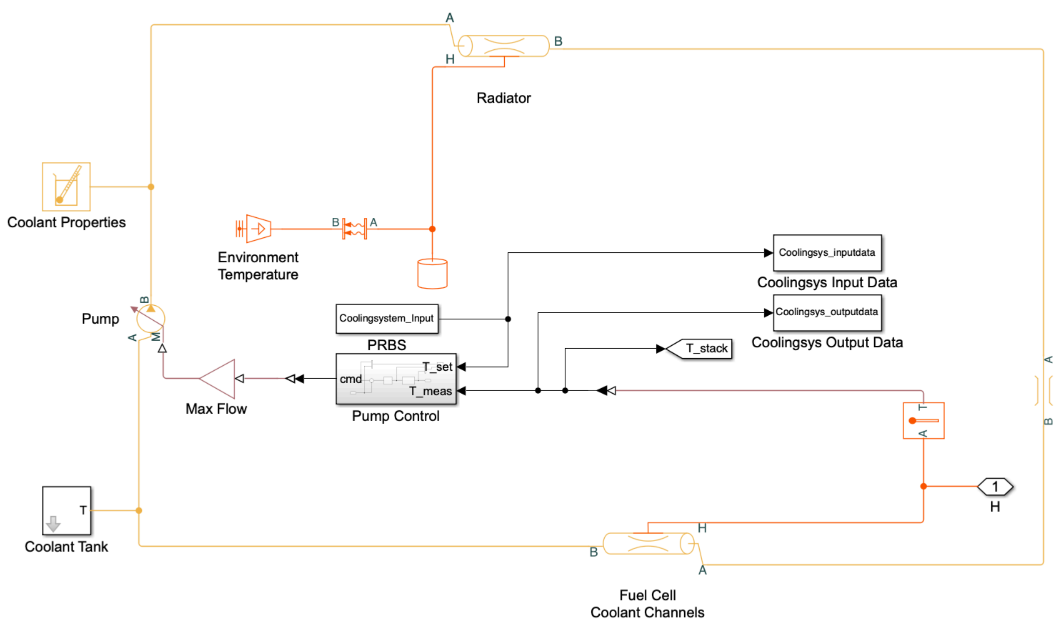

Unlike the original setting, the pump control block in the closed-loop identification is set to P mode instead of PI mode to maintain the pump operating around a desired setpoint of 80°C. The goal for the section is to model the cooling system while not interrupting the normal operations. A PRBS signal of 5% from the set point, which is 80°C, is introduced to generate set point variation. The output of the process is the temperature measurement response based on this input. Given the simulation data, we can subtract the mean temperature of datasets and then use the system identification toolbox in MATLAB for closed-loop identification.

The best fits for the estimated closed-loop models are shown on Fig. 16. “Coolingsys_P1” represents the first-order model, “Coolingsys_P2Z” represents the FOPTD model, “Coolingsys_P2” represents the second-order model, and “Coolingsys_P3Z” represents the second-order plus time delay model. The estimated parameters obtained from closed-loop identification are displayed in Table 7.

Figure 16. Best Fit for Estimated Closed-Loop Models Obtain from PRBS Setpoint with P = 0.1

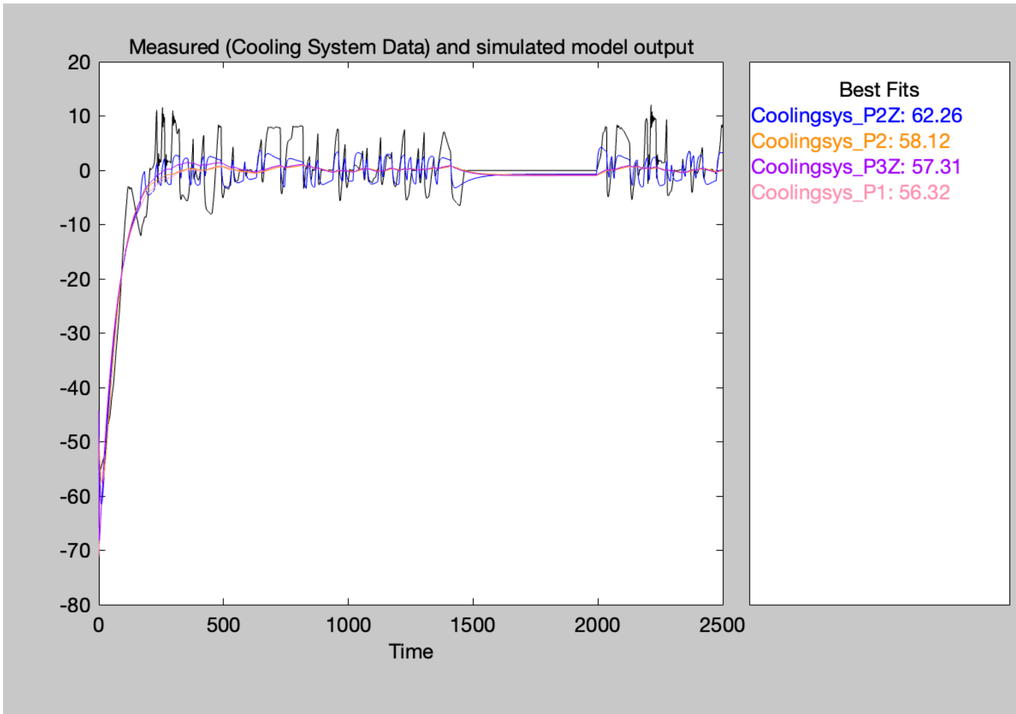

Table 7. Estimated Model Parameters for PEMFC Cooling System

Process Model	P Controller	Estimated Gain $\hat{K}$	Avg Time Constant τ sec	Time Delay θ sec	Damping Coefficient	Model Fit %
First-Order	0.1	4.2849	95.7388s	N/A	N/A	56.32
FOPTD	0.1	2.5644	2.0333s	456.9200s	N/A	62.26
Second-Order	0.1	3.2906	33.1530s	N/A	1.3932	58.12
SOPTD	0.1	3.5210	7.1475s	357.0200s	5.8620	57.31

From Table 7, we find that FOPTD and SOPTD usually have large time delay terms, which are impractical for real temperature systems. Usually, temperature is modeled by the first-order or second-order overdamped transfer function because no oscillation exists by nature. A large time delay may exist only when the thermocouple is far away from the system output. Considering the compact design of PEMFC, such a large time delay should not exist. Here both first-order and second-order models show similar accuracy and thus are all acceptable.

In the identification dataset, a step change from -70 to zero occurs within the first 100 seconds. Note that this is because we remove the average temperature from the actual measurement. This step change may affect the estimation accuracy. Hence, a trimmed dataset is created by excluding the step change, focusing instead on the more stable middle section of the data. Estimated closed-loop models were then generated based on this trimmed dataset. Using closed-loop transfer functions, process model parameters were estimated by applying the same technique. The best fit for the estimated closed-loop model is illustrated in Fig. 17, and the corresponding parameter estimates are summarized in Table 8.

Figure 17. Best Fit for Estimated Closed-Loop Models Based on Trimmed Dataset Using PRBS with P = 0.1

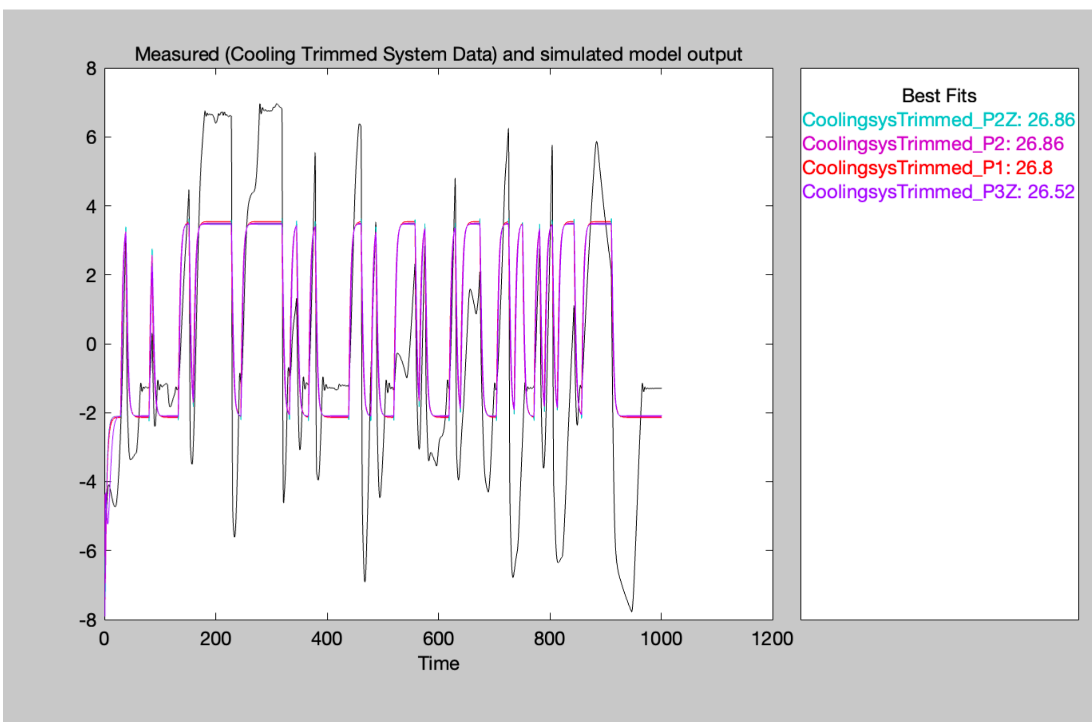

Table 8. Estimated Model Parameters Based on Trimmed Data for PEMFC Cooling System

Process Model	P Controller	Estimated Gain $\hat{K}$	Avg Time Constant τ sec	Time Delay θ sec	Damping Coefficient	Model Fit %
First-Order	0.1	24.4923	11.0441s	N/A	N/A	26.8
FOPTD	0.1	23.1950	8.6366s	0.4390s	N/A	26.8
Second-Order	0.1	23.3489	1.8585s	N/A	2.8239	26.8
SOPTD	0.1	22.6904	3.6037s	6.3672s	1.7771	26.8

Figure 17 shows a significant reduction in fitting accuracy, and Table 8 reveals substantial changes in all model parameters. This suggests that the cooling system in the PEMFC exhibits significant nonlinearity, and the large step change in the initial stage does indeed affect the estimated parameters. Given the low accuracy of model fits based on the trimmed dataset, we conclude that the model presented in Table 7 is more reliable.

5. Closed-Loop Identification of PEMFC Oxygen Supply System

The last subsystem modeled for the PEMFC is the oxygen supplier. The oxygen supply system consists of a compressor working at the proper speed to maintain the mass flow ratio between oxygen and hydrogen at a desired setpoint. The compressor is regulated by a P controller to facilitate closed-loop identification. There are two inputs to the compressor, including the oxygen excess ratio (OER) and stack current from the drive cycle. The system diagram for the compressor is shown in Fig. 18.

Figure 18. Oxygen Supply System Diagram

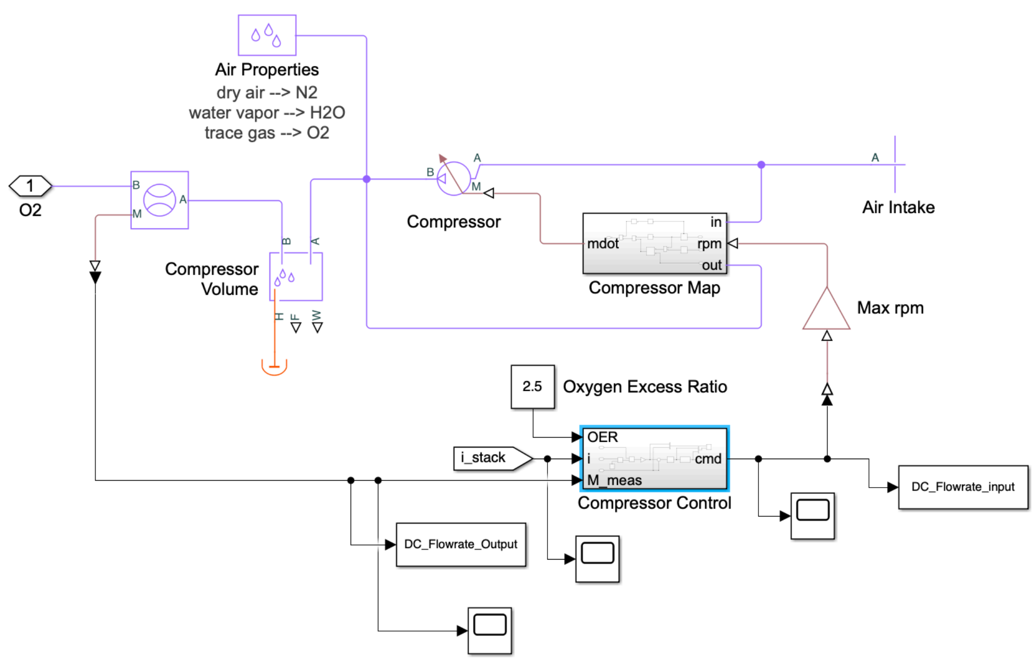

Fig. 18 shows that the input to the compressor will be the control action signal from the compressor control block, as its role is to maintain the proper speed of oxygen flow rate. The compressor output is feedback to the controller to form a close loop. Here the disturbance to the system is the current demand from a DC motor, which is controlled by pulse width modulation (PWM) provided by MATLAB. The system diagram for the DC motor is shown in Fig. 19 [5].

The DC system is controlled by an H-bridge that is responsible for generating a PWM signal. The DC motor operates at a rated speed of 2500 rpm and a rated voltage of 12 V. By using the current and motor speed data from the simulation, the power cycle can be deferred. The current data is provided by the current sensor, but voltage data must be obtained based on its proportionality to the RPM speed. To this end, a gain block based on the rated voltage and rated speed is introduced to convert RPM data to voltage data. The power cycle is the product of current and voltage, which will be then introduced into the PEMFC as the disturbance load. The input and output datasets from the closed-loop compressor system are collected to build the model. For this dataset, we only use the initial stage of the response signal representing the start of a car. After preprocessing and interpolating the data, the closed-loop models can be estimated based on the input and output signal. The best fits of these models are shown in Figure 20.

Figure 19. System Diagram for PWM-Controlled DC Motor

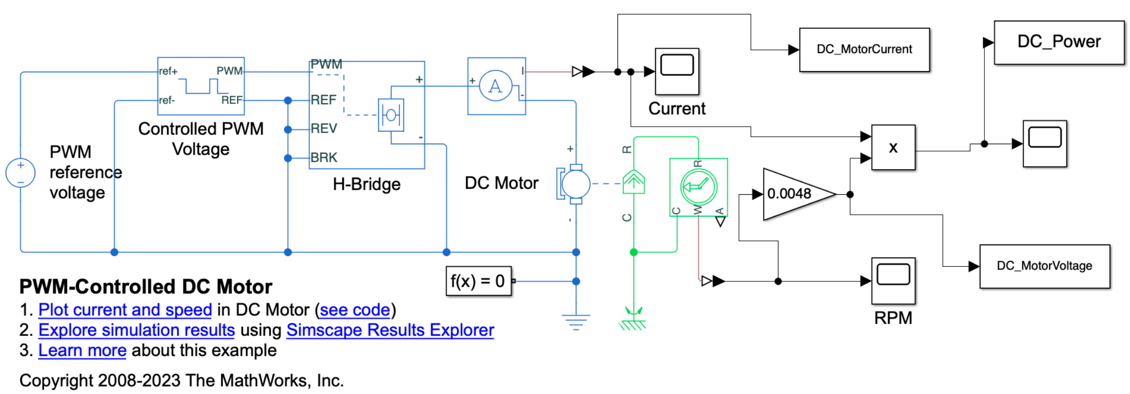

Figure 20. Best Fit for Estimated Closed-Loop Models for Oxygen Supply System with P = 10

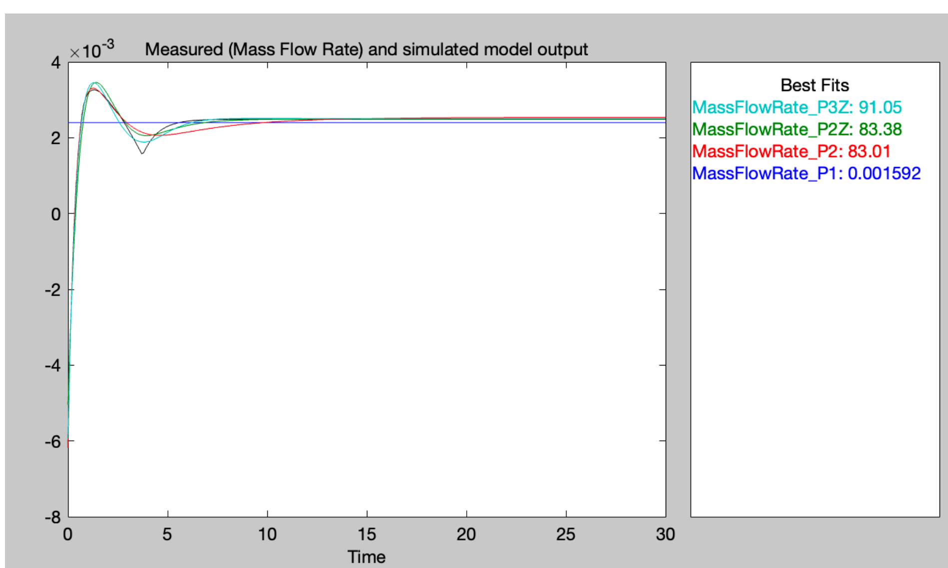

Since our simulation focuses solely on the vehicle start process, the sudden increase in power demand initially causes oscillations in the regulated OER. However, the system quickly approaches a steady state. We selected P = 10 instead of P = 0.1 to prevent insufficient power supply, which could otherwise prolong the vehicle's start process. The best model accuracy exceeds 90%, and the associated model parameters are summarized in Table 9.

Based on the estimated parameters, three out of the four models are viable candidates for the oxygen supply system. The first-order transfer function is excluded as it fails to capture the initial fluctuation, reflected by a poor fit of approximately 0%. The three models suitable for system design include the FOPTD, second-order, and SOPTD models. These models not only yielded reasonable parameters but also achieved best-fit values above 80%, indicating their ability to capture signal fluctuations effectively. Notably, they exhibit similar gain and time constant characteristics.

Given the model's fit results, we recommend using the SOPTD model for the oxygen supply system due to its superior performance and robustness.

Table 9. Estimated Model Parameters for PEMFC Oxygen Supply System

Process Model	P Controller	Estimated Gain $\widehat{K}$	Avg Time Constant τ sec	Time Delay θ sec	Damping Coefficient	Model Fit %
First-Order	10	0.0180	3.8195e+04 s	N/A	N/A	0.001592
FOPTD	10	0.0133	1.3961s	1.5862s	N/A	83.38
Second-Order	10	0.0135	1.2598s	N/A	1.7434	82.21
SOPTD	10	0.0133	0.6704s	2.2658s	1.1048	91.05

6. Summary & Conclusions

This report explores the modeling strategies for Proton Exchange Membrane Fuel Cells (PEMFCs) to improve their applications in heavy-duty vehicles. Our study applies a data-driven, closed-loop identification approach to model the PEMFC subsystems, including humidifier, cooling, and oxygen supplier within a Simulink-based simulation environment.

Our key findings and methodologies are summarized as below:

System Modeling: Various transfer function models (first-order, FOPTD, second-order, and SOPTD) were evaluated for accuracy in representing system dynamics under a closed-loop framework due to critical safety concerns.

Subsystem Analysis:

- **Humidifier:** FOPTD was the most effective model, demonstrating stable and accurate humidification control.
- **Cooling System:** Both first-order and second-order models were suitable; however, the presence of large time delays in certain models was deemed impractical.
- **Oxygen Supply System:** Second-order plus time delay models provided the best fit, especially under high controller gains necessary for vehicle start-up.

Data Collection: The data collected during the electric vehicle start-up process is particularly useful in modeling the transition performance of the transfer function model for PEMFC.

These findings underscore the importance of precise subsystem modeling to enhance PEMFC system efficiency, reliability, and safety.

Bibliography

[1] Daud, W. R. W., Rosli, R.E., Majlan, E. H., Hamid, S.A.A, Mohamed, R., Husaini, T. "PEM fuel cell system control: A review," *Renewable Energy*, *113*, 2017: 620–638.

[2] The MathWorks Inc. "PEM Fuel Cell System," Natick, Massachusetts: The MathWorks Inc. https://www.mathworks.com/help/simscape/ug/pem-fuel-cell-system.html, 2024.

[3] Forssell, U., & Ljung, L. "Closed-loop identification revisited," *Automatica*, *35*, 1999: 1215–1241.

[4] Mandloi, R., Shah, P. "Methods for closed loop system identification in industry," *Journal of Chemical and Pharmaceutical Research*, *7*, 2015: 892–896.

[5] The MathWorks Inc., "PWM-Controlled DC Motor," Natick, Massachusetts: The MathWorks Inc. https://www.mathworks.com/help/sps/ug/pwm-controlled-dc-motor.html, 2024.

About the Authors

Yang, Yu, PhD

Dr. Yu Yang received his BSc degree from Beijing Institute of Technology, Beijing, China, in 2004; his MSc degree from Zhejiang University, Hangzhou, China, in 2007; and his PhD from the Department of Chemical Engineering, University of Alberta, Edmonton, Canada, in 2011. He then became a postdoctoral associate at the Massachusetts Institute of Technology. He currently is an Associate Professor in the Department of Chemical Engineering at California State University, Long Beach (CSULB). His research interests include data-driven modeling, advanced process control, machine learning, global optimization under uncertainty, and the analysis and design of renewable energy systems.

Yeh, Hen-Geul, PhD

Dr. Hen-Geul Yeh received his BSc degree in engineering science from National Chen Kung University, Taiwan, ROC, in 1978; and his MSc degree in mechanical engineering and his PhD in electrical engineering from the University of California, Irvine, in 1979 and 1982, respectively. Since 1983, he has been with the Electrical Engineering Department at CSULB and has served as the Department Chair from 2016 to 2022. In addition to his technical and engineering excellence, he was selected as a NASA JPL Summer Faculty Fellow twice, in 1992 and 2003, and the Boeing Welliver Faculty Fellow in 2006. His research interests include DSP/Communication/Control algorithms development using MATLAB, and their implementation using FPGA and digital signal processors with applications in communication systems, smart grids, optimization, controls, and electrical event detection, with a focus on real-time digital signal processing, Wi-Fi and Wi-MAX, adaptive systems, and mobile communication in multipath fading channels. He has published over 100 research papers on signal processing, communications, controls, and smart grids.

Bryan Aguirre

Bryan Aguirre holds a B.S. in Biochemistry from California State University, Los Angeles (CSULA) and earned an M.S. in Chemical Engineering from CSULB. His research interests are in the renewable energy and biotechnology sectors.

MTI FOUNDER

Hon. Norman Y. Mineta

MTI BOARD OF TRUSTEES

Directors

Karen Philbrick, PhD
Executive Director

Hilary Nixon, PhD
Deputy Executive Director

Asha Weinstein Agrawal, PhD
Education Director
National Transportation Finance Center Director

Brian Michael Jenkins
Allied Telesis National Transportation Security Center

MINETA TRANSPORTATION INSTITUTE